ACS APPLIED MATERIALS & INTERFACES

www.acsami.org

Research Article

Role of Trapped Molecules at Sliding Contacts in Lattice-Resolved Friction

Miljan Dašić,* Roy Almog, Liron Agmon, Stav Yehezkel, Tal Halfin, Jürgen Jopp, Assaf Ya'akobovitz, Ronen Berkovich,* and Igor Stanković*

Cite This: *ACS Appl. Mater. Interfaces* 2024, 16, 44249−44260

Read Online

ACCESS | Metrics & More | Article Recommendations

ABSTRACT: Understanding atomic friction within a liquid environment is crucial for engineering friction mechanisms and characterizing surfaces. It has been suggested that the lattice resolution of friction force microscope in liquid environments stems from a dry contact state, with all liquid molecules expelled from the area of closest approach between the tip and substrate. Here, we revisit this assertion by performing in-depth friction force microscopy experiments and molecular dynamics simulations of the influence of surrounding water molecules on the dynamic behavior of the nanotribological contact between an amorphous SiO_2 probe and a monolayer MoS_2 substrate. An analysis of simulation and experimental stick−slip patterns demonstrates the entrapment of water molecules at the contact interface. These trapped water molecules behave as an integral component of the probe and participate in its interaction with the substrate, affecting the dynamics of the probe and preventing long slips. Significantly, surrounding water from the capillary or layer exhibits a replenishing effect, acting as a water reservoir during sliding. This phenomenon facilitates the preservation of lattice-scale resolution across a range of applied normal loads.

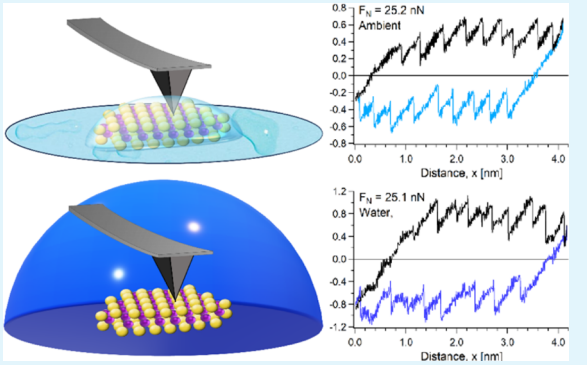

KEYWORDS: *molybdenum disulfide, water, friction, stick−slip, friction force microscopy, molecular dynamics*

INTRODUCTION

Water can effectively perform as a lubricant under certain conditions, yet it is not a suitable lubricant in many technological applications, since it is easily expelled from the contacts.[1,2] Such scenarios can be encountered during the synthesis of ionic liquid lubricants, where water migrates toward surfaces,[3−6] also in case of solid lubricants,[7] or in case of humidity condensation.[8,9] Although the accepted notion states that a direct solid−solid contact stays dry under an applied load, the presence of single molecules trapped between sliding surfaces has been suggested.[10−13]

Atomic force microscopy (AFM) can measure frictional dynamics at the nanoscale in different environments, such as in air,[14] liquids,[15] and ultrahigh vacuum (UHV).[16] In a typical friction force microscopy (FFM) experiment, a sharp AFM tip is elastically driven across a solid surface, while capturing its interaction with single asperities across atomical corrugation in the nanometer range.[17] Throughout this process, dissipation mechanisms at lattice resolution can be accessed by recording friction forces at the interface over time, while creating lateral friction loops and maps. Measuring at the lattice resolution, the friction signal manifests binding and unbinding across atoms at the contacting surfaces, with a stick−slip pattern.[18,19]

Experimentally achieving high subnanometer resolution under UHV is highly demanding, while measuring in ambient conditions can involve the possible presence of contaminants and the formation of water bridges (i.e., capillary condensation) between the tip and the surface.[2,19−21] The latter was shown to be eliminated in case the measurement is performed in liquid surroundings[17,22,23] when the probe tip and the sample are completely immersed in liquid.

FFM measurements and molecular dynamics (MD) simulations of a silicon AFM probe scanning across a graphene surface revealed that a high-resolution signal obtained in the liquid environment is comparable to the signal obtained in UHV, albeit with noisier results due to the thermal collisions of water molecules with the AFM tip.[17] The MD simulations showed that this equivalency resulted from the removal of all water molecules from the tip−sample gap, as the tip engaged in full contact (while breaking hydration layers) with the sample,

Received: May 19, 2024
Revised: July 22, 2024
Accepted: July 24, 2024
Published: August 6, 2024

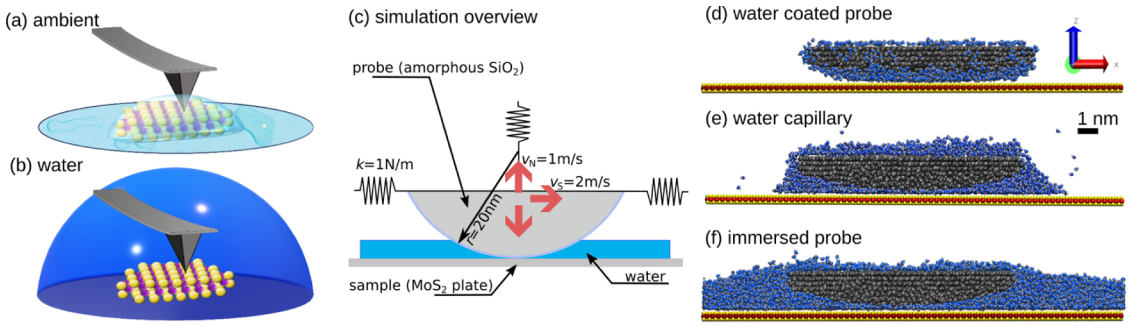

Figure 1. Schematic illustration of the experimental FFM setup in (a) ambient conditions (air, room temperature). At RH ≈ 35−40%, a thin (molecular) layer of water condenses on the surface. (b) Water (double distilled) layer completely immersing the sample and the cantilever. (c) Schematic representation of the implemented simulation setup, which is designed following the experimental FFM setup shown in panels (a, b) of this figure. The values of the parameters defining the simulation setup are velocities v_N = 1 m/s and v_S = 2 m/s that are related to the force−distance and sliding simulations, respectively; spring stiffness coefficient k = 1 N/m is the same for the elastic springs attached to the probe in all three Cartesian directions (i.e., in x−, y−, and z− directions); radius r = 20 nm defines the curvature of the probe. Illustration of different water setups: (d) configuration snapshot in case of a water coated probe, (e) probe surrounded by a water capillary, and (f) probe immersed in a continuous layer of water.

thus forming a completely dry contact. Nevertheless, recent FFM studies on NaCl crystal in ethanol surroundings suggested that under the assumption that no solvent molecules interfere at the contact, the liquid environment creates different thermodynamic conditions from those in UHV.[24] In the liquid environment, the solvent serves as a heat reservoir, maintaining isothermal conditions. Consequently, there was an increase in lateral stiffness,[23,24] which remained hardly unchanged in UHV,[25] but exhibited longer slip-length dynamics[26] that were not observed in the liquid surrounding.[24] It was also shown that the presence of adsorbed molecules could contribute to enhanced energy dissipation mechanisms during kinetic friction.[13]

In order to deepen our understanding of these differences, we explore here the influence of water-moderated friction on the sliding contact between molybdenum disulfide (MoS_2) monolayer and silicon/silica (Si/SiO_2) tip in two cases: in ambient conditions, i.e., in air with ≈35−40% relative humidity (RH), and with the tip being fully immersed in double distilled water. The FFM measurements were complemented by MD simulations that provided additional information and deepened our understanding of the underlying mechanisms, cf. Figure 1.

MoS_2 belongs to a chemical family of transition metal dichalcogenides (TMDs).[27] It is known for its remarkable mechanical properties (such as the high stiffness and extremely low friction coefficients), and it is widely explored in nanotribological studies.[23,27−30] Additionally, the quality of MoS_2 as a solid lubricant strongly depends on the level of air humidity from a purely tribological perspective, where a humid environment leads to an increased friction coefficient.[28] To elucidate the influence of water on the nanoscale tribological properties of monolayer MoS_2, we performed a synergistic investigation that combines FFM experiments with MD simulations. Such a comprehensive approach, encompassing both water capillary environments and full immersion scenarios of the AFM probe, yielded invaluable insights into the interplay between water and nanotribological behavior of MoS_2. First and foremost, we investigate whether a setup with a thin water layer formed due to condensation or a probe fully immersed in water influences the lateral interaction between the Si/SiO_2 probe and the monolayer MoS_2. We investigate the presence of water molecules and their impact on the lateral interaction between the Si/SiO_2 probe and the monolayer MoS_2. A scenario is outlined in which the trapped water molecules become an integral parameter in the overall tribological interaction. Different friction coefficients and local stiffness, as well as different slip-length dynamics, manifest such an impact. Overall, the combined experimental and simulation approaches offer a comprehensive understanding of the intricate dynamics governing the slip events, thus providing valuable insights into the tribo-system's behavior under varying operating conditions.

METHODS

Experimental Methods. The FFM measurements were performed in ambient conditions (i.e., air; room temperature; RH ≈ 35−40%), and in water (double distilled), where the cantilever and surface were fully immersed, as illustrated in Figure 1(a,b), respectively. In the presence of vapor (in this study, the water moisture), local pressure and temperature can induce condensation.[31] The experiments were performed with an Asylum Research Cypher-ES AFM (Oxford Instruments) in the contact mode using silicon probes (SNL-D, Bruker), with a normal spring constant of $k_N \approx 0.065$ N/m and a lateral sensitivity of α = 96.7 nN/V. The lateral sensitivity was measured with the wedge calibration method.[32,33] Fresh new cantilevers were used for the measurements. After being mounted and sealed within the AFM measuring chamber, extensive scans over tens of micrometers were conducted to identify the desired measurement regions within the MoS_2 flakes precisely. During this process, the surfaces of the tips were gently cleaned mechanically. Although the tip is made of silicon, when exposed to ambient air, it gets oxidized and covered with a thin (1−2 nm) layer of amorphous SiO_2. Accordingly, we refer to the tip as Si/SiO_2, and in the MD simulations, the tip's surface is modeled as amorphous SiO_2. For further details regarding the synthesis and characterization of the MoS_2 monolayers (on a silicon wafer), cf. ref 23. Figure 2 presents two micrographs of MoS_2 flakes. Before every experiment, the MoS_2 monolayer was rinsed with acetone and ethanol.

The measurements were performed by scanning back and forth across the distance of 5 nm at 90° scan angle (perpendicular to the axis of the cantilever), collecting friction loops at a constant scanning rate of 2 Hz. To account for the effect of crystallographic orientation on the MoS_2-tip interaction,[30,34,35] the FFM measurements were conducted across a statistically significant sampling of MoS_2 flakes and orientations, thereby averaging out inherent local variations in frictional behavior.[23] During the measurements, external normal loads of F_N = {4.2, 8.4, 12.6, 16.8, 21.0, 25.2, 29.5} nN were applied (with the corresponding number of slip events at each load of n = {501, 996, 518, 269, 456, 1640, 529}) in the ambient conditions (air);

https://doi.org/10.1021/acsami.4c08226
ACS Appl. Mater. Interfaces 2024, 16, 44249−44260

Figure 2. Optical images of MoS_2 flakes.

while normal loads of F_N = {3.1, 6.3, 9.4, 12.6, 15.7, 22.0, 25.2} nN were applied (with the corresponding number of slip events at each load of n = {423, 225, 239, 820, 498, 731, 843}) in water surroundings. Some of the friction traces exhibit strengthening of the friction signal with the sliding distance (sometimes referred to as "tilted loops"),[36] which is associated with puckering,[37] and other underlying interfacial mechanisms.[38−40] Accordingly, the friction forces were analyzed using the same approach reported in the literature, where tilted friction loops were observed, where the friction signal was taken as half of the difference between the slip forces in the forward and the backward scans.[39,41−44] Local stiffnesses were obtained by taking the slopes in the stick phase in the friction traces, and slip lengths were calculated using Hooke's law.[24,26,45] All these parameters were assembled into distributions, from which their median and interquartile ranges were calculated to provide their characteristic values. IGOR Pro 6.3.7.2 (WaveMetrics) and MATLAB (R2021b) software were used to process and analyze the force spectroscopy data.

Interaction Model. A classical molecular dynamics method enabled the consistency with experimental investigation and the capture of relevant interatomic interactions. As a result, we could properly model the system's length and time scales. We employed an atomistic model to describe the interactions of all atoms in the system. Intramolecular interactions between the water molecule are modeled with the SPC potential,[46,47] with LJ parameters σ_O = 3.166 Å, ϵ_O = 0.155 kcal/mol, r_{OH} = 1 Å, H−O−H angle 109.47°, oxygen charge −0.8476e and hydrogen charge 0.4238e. Interactions between the water and the solids are modeled as nonbonded and described via the Lennard-Jones (LJ) and Coulombic potentials. In the case of the molybdenum atom in MoS_2, LJ parameters were taken at σ = 4.43 Å, ϵ = 0.116 kcal/mol, and charge 0.5e, while for sulfur, σ = 3.34 Å, ϵ = 0.4983 kcal/mol, and charge −0.25e.[48] In the case of the oxygen atom in SiO_2, LJ parameters were taken at σ = 3.826 Å, ϵ = 0.15 kcal/mol, and charge −0.45e, while for silicon, σ = 3.112 Å, ϵ = 0.3 kcal/mol, and charge 0.9e.[49] We distinguish the oxygen atoms in the SiO_2 probe from the ones in the water molecules since they have slightly different LJ parameters (ϵ, σ). Within the implemented description of the system, each of the atomic types is defined by its LJ parameters and its charge. The LJ parameters defining the pair interaction of two atoms belonging to the same type (labeled as α) are ($\epsilon_{\alpha\alpha}$, $\sigma_{\alpha\alpha}$), while all the atoms belonging to the same type have the same charge q_α. Cross-interaction parameters between different atomic types are calculated using the Lorentz−Berthelot mixing rules,[50,51] i.e., $\epsilon_{\alpha\beta} = \sqrt{\epsilon_{\alpha\alpha}\epsilon_{\beta\beta}}$, $\sigma_{\alpha\beta} = \frac{\sigma_{\alpha\alpha} + \sigma_{\beta\beta}}{2}$.

Water is in the liquid state, meaning that the H_2O molecules are not ordered in any regular structure. The studied temperature of T = 350 K in sliding simulations belongs to the temperature range corresponding with the liquid state of water. The relative positions of atoms in the substrate and the probe are fixed. The curvature of the probe is defined by its radius of 20 nm, the in-plane size of the substrate is 24 × 24 nm^2, and the periodic boundary conditions (PBC) are applied in the substrate plane (i.e., in the xy plane of the Cartesian coordinate system).

All MD simulations have been performed using the LAMMPS software package,[52] with time steps of 2 fs and a Nose-Hoover thermostat set to the chosen temperature. We used the particle−particle particle-mesh (PPPM) solver[53] for handling the long-range electrostatic interactions with the accuracy (i.e., the desired relative error in forces) of 10^{-5}, and LJ interactions had a cutoff distance of 12 Å.

Simulation Setup. A schematic representation of the developed MD simulation setup is shown in Figure 1(c). An amorphous SiO_2 probe with a curvature radius of r = 20 nm is placed above the sample (within the framework of this study, that is a monolayer crystalline MoS_2 plane). The amorphous SiO_2 probe was obtained via a melt-quench technique: by heating the α-quartz at T = 1000 K, and then quenching it at T = 300 K. The probe was spherically shaped by cutting it correspondingly. We designed a water coating by placing N = 1200 water molecules under the probe on the planar substrate, see Figure 1(d), thus obtaining a water coated probe. When the number of water molecules is higher (N = 6415), the probe is surrounded by a water capillary, see Figure 1(e). The layer of water in which the probe

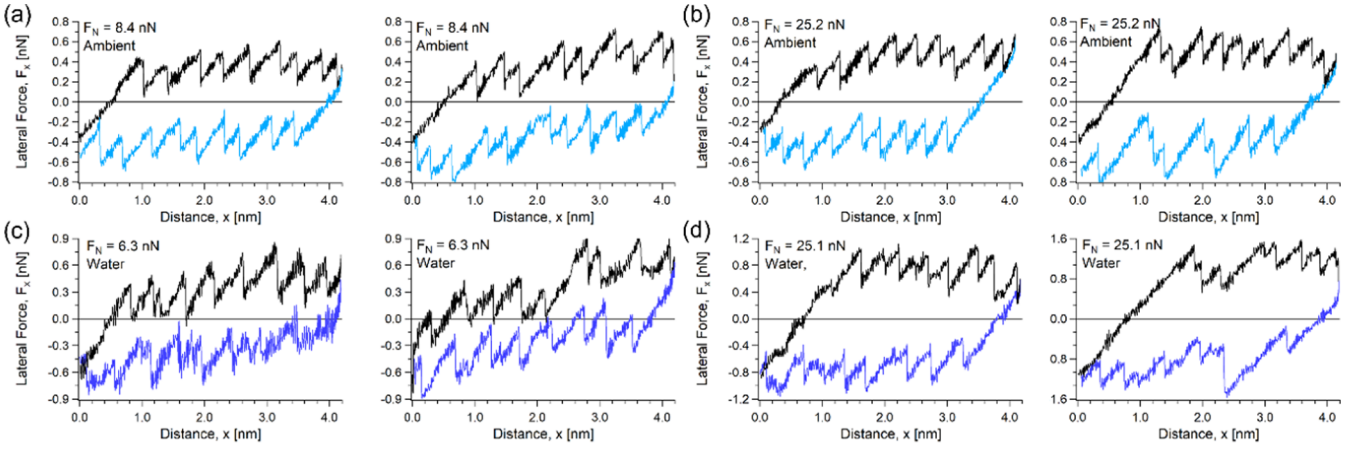

Figure 3. Representative Si/SiO_2−MoS_2 experimental friction loops displaying the stick−slip pattern measured in air (black-light blue) under a load of 8.4 nN (a), and 25.2 nN (b), and in water (black-blue) under a load of 6.3 nN (c), and 25.1 nN (d).

https://doi.org/10.1021/acsami.4c08226
ACS Appl. Mater. Interfaces 2024, 16, 44249−44260

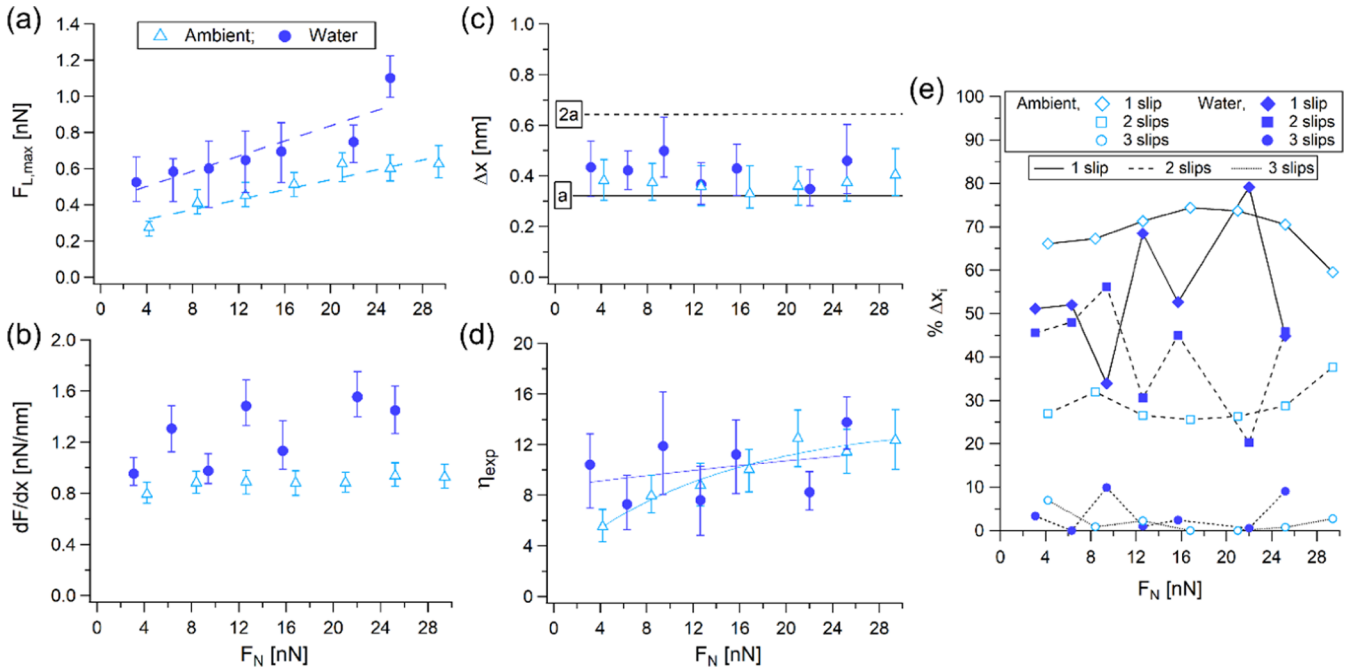

Figure 4. Frictional behavior of Si/SiO_2−MoS_2 with the normal load measured in ambient conditions (empty light blue triangles) and in water (blue circles). (a) Lateral slip forces with linear fits (dashed lines). (b) Local shear stiffness. (c) Slip lengths. The continuous and the dashed lines correspond to the values of the single and double lattice constants. (d) PT parameter η_{exp}, with lines drawn to guide the eye. (e) Percentage of the slip length populations denoted by continuous (single slip events), dashed (double slip events), and dotted (triple slip events) lines.

is fully immersed, see Figure 1(f), consists of N = 24,000 water molecules. The fully immersed probe and capillary scenarios help us understand the effects of significant water presence, while the third scenario examines the impact of a minimal amount of water. These setups allow us to investigate the role of water quantity and distribution on the structure−property relationships in the studied nanotribological system. The probe is connected to the support via harmonic elastic springs in all three orthogonal directions (i.e., in x-, y-, and z- directions), to measure the lateral and normal forces similar to the FFM experiment. The support is pulled at a constant velocity in a direction parallel (x) or orthogonal (z) to the substrate (the xy plane). The probe has a spring stiffness of k = 1 N/m in all three orthogonal directions.

We performed MD sliding simulations at the temperature of T = 350 K since experimental measurements are usually performed at much lower velocities than those achievable in MD simulations. In part, we tried to compensate for high velocity in MD simulations by increasing the mobility of water molecules. The elevated temperatures result in the water molecules having a higher probability of leaving the moving contact, compared to the room temperature of T = 300 K. We moved the probe: (i) orthogonal to the MoS_2 sample with a velocity of v_N = 1 m/s (i.e., along the z- direction), and (ii) parallel to the MoS_2 sample with a lateral sliding velocity of v_S = 2 m/s; the directions and values of the two imposed velocities are indicated in Figure 1(c).

RESULTS

Effect of the Normal Load on the Stick−Slip Friction in FFM Experiments. Figure 3 shows several FFM friction loops measured at low and high loads under ambient conditions (black and light-blue, Figure 3(a,b)), and when fully immersed in water (black and blue, Figure 3(c,d)). Friction loops show the stick−slip friction pattern, in which more than single slip events can be observed. We characterized the frictional behavior of the two systems in terms of the medians and interquartile ranges (IQR) of the slip forces, $F_{L,max}$, and local stiffness, given by their slopes, dF_x/dx, under each applied normal load. Figure 4(a) plots $F_{L,max}$ with the change of normal load F_N, fitted with a linear form of Amontons' law: $F_{L,max} = F_{L,0} + \mu F_N$, where $F_{L,0}$ defines the frictional force at zero normal force (which is associated with adhesion), and μ represents the friction coefficient. From the fitting of the experimental data, see the dashed lines in Figure 4(a), the following values were obtained: $F_{L,0}^{ambient} = 0.26 \pm 0.04$ nN, and $\mu_{ambient} = 0.014 \pm 0.002$ for the lateral interaction in ambient conditions, and $F_{L,0}^{water} = 0.42 \pm 0.08$ nN, and $\mu_{water} = 0.021 \pm 0.005$ in water. When we compare the measurements in ambient conditions and in water, it is interesting to observe that both the friction force at zero normal force ($F_{L,0}$), and friction coefficient (μ) differ. Based on this behavior, the friction interaction in water appears to be somewhat stronger, yet the last force point at 25.2 nN numerically affects the fitted values. Excluding this point results with $F_{L,0}^{water} = 0.50 \pm 0.01$ nN, and $\mu_{water} = 0.012 \pm 0.001$, which is very close in value to the fitted friction coefficient at ambient conditions. This indicates that the local lubrication conditions at the contact may not be so different in both cases, where several water molecules may be trapped in the sliding contact.

Figure 4(b) illustrates that the local shear stiffness under ambient conditions is narrowly distributed around approximately 0.9 nN/nm, with no clear trend. However, in water it increases with the normal load, from 0.95 to 1.45 nN/nm, exhibiting significant fluctuations. It is interesting to compare the observed behavior in water to a similar system measured in ethanol surroundings. Similar FFM experiments on monolayer MoS_2 with the same brand of the cantilever in ethanol surroundings reported values close to those measured in water (i.e., $F_{L,0}^{ethanol} = 0.503$ nN, $\mu_{ethanol} = 0.019$).[23] The consistent behavior observed in analogous sliding contacts under different environments indicates not only the explicit influence of water molecules trapped at the contact but also the role of the external environment surrounding the contact area.[24]

https://doi.org/10.1021/acsami.4c08226
ACS Appl. Mater. Interfaces 2024, 16, 44249−44260

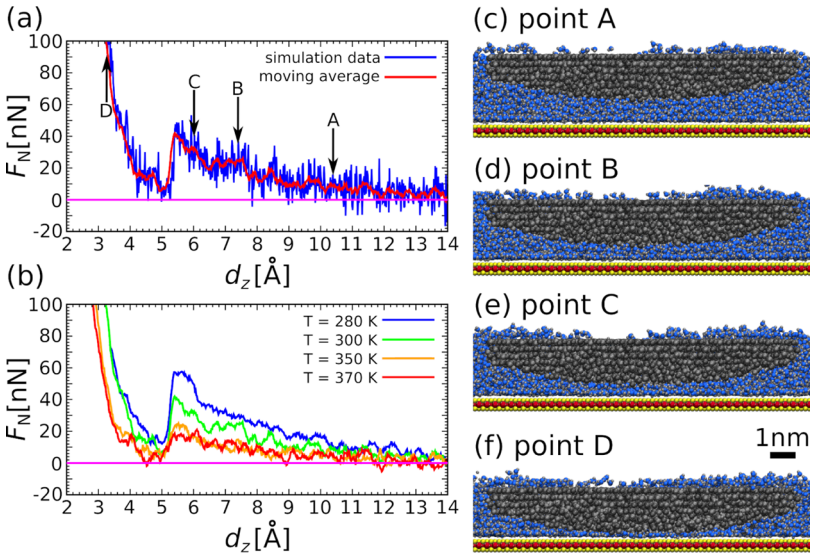

Figure 5. Force−distance $F_N(d_z)$ characteristic simulated at the temperature of T = 300 K. (a) The blue line corresponds to the raw MD simulation data, while the red line represents the moving average (0.1 Å window). (b) The force−distance characteristic at T = 280, 300, 350, and 370 K. The cross sections through the middle of the probe at the characteristic points (c−f) correspond to the respective points in panel (a).

To extract more information on the effect of the different environments, we calculated the slip length, labeled as Δx, which is defined as the distance between slip events. The median slip lengths at each applied load, for both air and water, are shown in Figure 4(c). It can be observed that the measured slip lengths are slightly larger than a single lattice constant (a_{MoS_2} = 3.212 Å[54]), but smaller than two lattice constants. The IQRs that characterize the shape of the slip length distributions in Figure 4(c) indicate that several slip length populations are involved. These deviations from the exact value of the lattice constant emerge from the way in which the slip length is calculated, i.e., by dividing the force drop at the slip event by the local stiffness.[24,26,45] Hence, experimental errors in the evaluations of these parameters (related to instrumental effects and anisotropy-associated averaging) lead to these small differences between the calculated and the actual slip lengths.

Multiple slip length dynamics can be described with the Prandtl-Tomlinson (PT) parameter and the dissipative state of the system.[24,26,45,55,56] The PT parameter[57,58] is a dimensionless number, defined within the PT model.[59] It describes the tip−sample sliding interaction through the ratio between the amplitude of the tip−sample interaction and the elastic energies, $\eta = (2\pi/a) \times 2U_0/K_{eff}$, where a is the lattice periodicity (constant), U_0 is the corrugation interaction amplitude, and K_{eff} is the effective spring constant that represents the elastic interaction at the sliding contact. Since U_0 and K_{eff} are unknown, the PT can be redefined in terms of the experimental measurables,[25] i.e., in terms of $F_{L,max}$ and dF_x/dx, as $\eta_{exp} = (2\pi/a)(dx/dF_x)F_{L,max} - 1$. The calculated η_{exp} at the different loads (Figure 4(d)), shows an increase from ≈4 to ≈12 in air, and large fluctuations between ≈7 and ≈13 with a slight increase trend, for water. Such large values mean that the corrugation interaction energy is larger than the elastic energy at the contacts, which is associated with the multiple slip dynamics.[24,26,45,55,56]

We distinguish between the slip lengths that distribute into single, double, and triple slip events, i.e., occurring over one, two, or three lattice constants, and the extent to which these jumps take place. Figure 4(e) plots the percentage of these slip events at every applied normal load. During low-load sliding, a higher occurrence of single-slip events is observed in ambient conditions than in the aqueous environment. This disparity diminishes for the applied loads exceeding 8 nN, due to the emergence of pronounced fluctuations within the measured slip lengths for water. While the dynamic in water is more erratic, in ambient conditions we can notice a larger number of single-slip events compared to the double-slip events, which are more frequent than the three-slips, cf. Figure 4(e). With an increase of the load, the fraction of the single-slip events increases from ≈67 to ≈74% and then reduces to ≈59%. Oppositely, the fraction of the double-slip events increases from ≈26 to ≈38%. The three-slip population demonstrates an intriguing behavior: it peaks at the lowest load, constituting the largest proportion of ≈7%, then it quickly decays to zero, and afterward, it slightly grows at high loads to ≈3%. The increase of the two- and three-slip events with the normal load is expected, due to the changes in the η parameter with the damping state of the system.[24,26,45,56] The relatively high percentage of the three-slip events at the applied normal load of 4 nN (at η_{exp} = 5.5) in ambient conditions, can indicate the possible presence of trapped condensate water molecules in the contact, which are pushed out with the increase of the local pressure at higher loads.

MD Simulations: Force−Distance Characteristics. Typically, the inefficiency of water as a lubricant is attributed to its limited resistance to being squeezed out. Therefore, gaining insights into the normal forces that the water layer can sustain before becoming dislodged from the contact is crucial. Using MD simulations: the temperature, the probe-substrate distance and the resulting normal load are followed, together with the structure of the confined water layer. Figure 5(a) shows the force−distance evolution $F_N(d_z)$ at T = 300 K including the raw simulation data (solid blue line) and the moving average (solid red line). The values of F_N remain under 10 nN at high probe-sample distances, i.e., d_z > 10 Å. As the gap decreases, the normal force steadily increases at lower probe-sample distances, i.e., d_z < 10 Å. Point A in panel (a) of Figure 5 corresponds to the roughly three layers of water molecules (i.e., hydration layers) confined in the probe-sample

https://doi.org/10.1021/acsami.4c08226
ACS Appl. Mater. Interfaces 2024, 16, 44249−44260

gap. We measure the number of confined water layers based on the gap width versus the diameter of the water molecule. The distinctive steps are visible, cf. points B and C in Figure 5(a). At these steps, the final hydration layers exert resistance before being expelled from the gap by the probe. As a result, the normal force increases at these points as the number of layers decreases from three layers to two and further, from two layers to a single layer. This behavior is reminiscent of previously seen behavior in the studies on ionic liquids and alkanes.[60−63] The hydration layers are broken at somewhat low normal loads, which agrees with previous results obtained with frequency-modulation AFM.[64] Distance points in Figure 5(a) labeled as A, B, C, and D, correspond to the configuration snapshots provided in the panels (c−f) of Figure 5, respectively. We observe that the water molecules remain trapped in the space between the probe and the substrate after a single full layer gets squeezed out, cf. panel (f) of Figure 5. For d_z < 5.0 Å, the normal force F_N further increases with the reduction of the probe-substrate gap distance d_z. After the point of local minimum of the normal force F_N, i.e., at the distance $d_z \approx$ 5.0 Å, cf. Figure 5(a), the normal force F_N steadily increases again, as the remaining trapped water molecules get squeezed out. The probe-substrate (i.e., SiO_2−MoS_2) direct contact is detectable from the final and steep increase of the normal force F_N, cf. point D in Figure 5(a).

In their MD simulation study, Vilhena et al.[17] reported that the normal force required to break the first hydration layer was 2 nN for $S_{contact}$ = 0.8 nm^2 diamond tip on graphene at T = 300 K, i.e., $F_N/S_{contact}$ = 2.5 GPa. In our current MD simulations, the estimated contact surface is larger (20 nm^2), and the maximal load is 40 nN. The resulting load-bearing capacity of the first hydration layer is $F_N/S_{contact}$ = 2 GPa, which is in proximity to the result of Vilhena et al.[17]

The effect of temperature on the force−distance characteristic of the studied nanotribological system is shown in Figure 5(b). Force−distance curves were obtained at temperatures below the water's boiling point, i.e., T = {280, 300, 350, 370} K. As the temperature increases, there is an apparent decrease in the normal force F_N. Also, we observe that the normal force minima becomes more profound, while simultaneously the point of the probe-sample minimal distance gets delayed with an increasing temperature, cf. Figure 5(b). We should note that according to our MD simulation setup, the probe and substrate atoms cannot change their relative positions. Simultaneously, the mobility of water molecules increases with the temperature. We observe that, at higher temperatures, fewer water molecules are trapped in the probe-sample contact area. Elevation of temperature results in kinetic energy increase of water molecules confined within the microscopic roughness of the amorphous SiO_2 surface, facilitating their escape from the roughness. The effect of temperature and the resulting mobility of water molecules is manifested in the cross-section of the system parallel to the MoS_2 plate at d_z = 3.2 Å in Figure 6. Configuration snapshots show an evident decrease in the number of water molecules (colored in blue) trapped inside the probe-sample gap, with the temperature increase. Simultaneously, with increasing temperature the diameter of the void space under the probe increases, and the density of trapped water molecules decreases. We observe in the temperature range T = 280 K to T = 300 K about 20 water molecules less in the gap, while in both ranges 300−350 and 350−370 K, there were roughly further 60 molecules less, for each increment of the temperature.

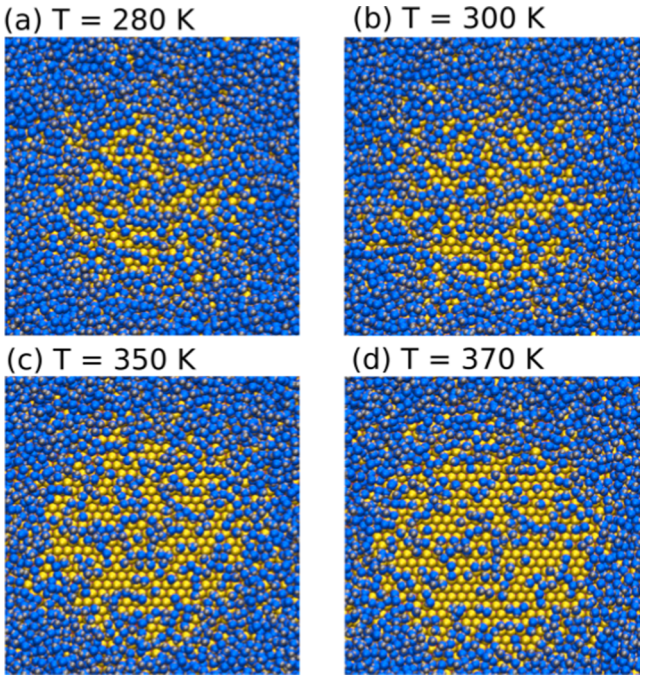

Figure 6. Cross sections of the probe-sample contact (a−d) show water molecules above MoS_2 plate at T = 280, 300, 350, and 370 K for d_z = 3.2 Å, respectively. The water molecules (blue oxygen) and substrate (yellow sulfur) are visible. The effect of temperature is visually noticeable as the area comprising MoS_2 surface atoms increases with temperature increase.

Simulated Dynamics of the AFM Probe. To examine the interactions between water, the amorphous probe, and the substrate, and to explore potential mechanisms leading to the lattice-resolved stick−slip friction, we conducted FFM MD simulations with explicit water. One could argue that the water molecules trapped under the AFM probe will leave once the sliding starts and that only the atoms of the two solids will remain in contact. We investigate this point in Figure 7(a) by following the evolution of the probe-substrate gap Δz_{gap} with the sliding distance Δx. The results are presented as the difference between the current and the initial positions. Accordingly, Figure 7 illustrates the extension of the spring in the sliding direction due to the lateral force, as well as the spring release in the direction of the substrate, during the sliding process. In our MD sliding simulations, the probe covered a distance of Δx = 15 nm, corresponding to roughly 46 MoS_2 hollow (i.e., Mo top) site distances. At the onset of sliding, the AFM probe rapidly descends toward the substrate, as water molecules get squeezed out, cf. Δx < 3 nm, cf. Figure 7(a). For the case of both the water coated and the capillary water systems, $x \approx$ 3 nm corresponds to the length of the initial stick. After the initial descent, the probe's elevation does not change in immersed and capillary water systems. Further stepwise descends are visible for the water coated probe at $x \approx$ {3, 6, 9} nm. Such behavior could be attributed to the individual water molecules that are squeezed out or displaced within the probe-substrate gap during the shear. A contact point between the atoms of the probe and the substrate devoid of water molecules, i.e., in case of a "dry contact", would not exhibit a reduction of the probe-to-substrate distance during the sliding process since in all three systems probe is geometrically equivalent. Without water molecules trapped in the probe-substrate gap, all three systems would exhibit an

https://doi.org/10.1021/acsami.4c08226
ACS Appl. Mater. Interfaces 2024, 16, 44249−44260

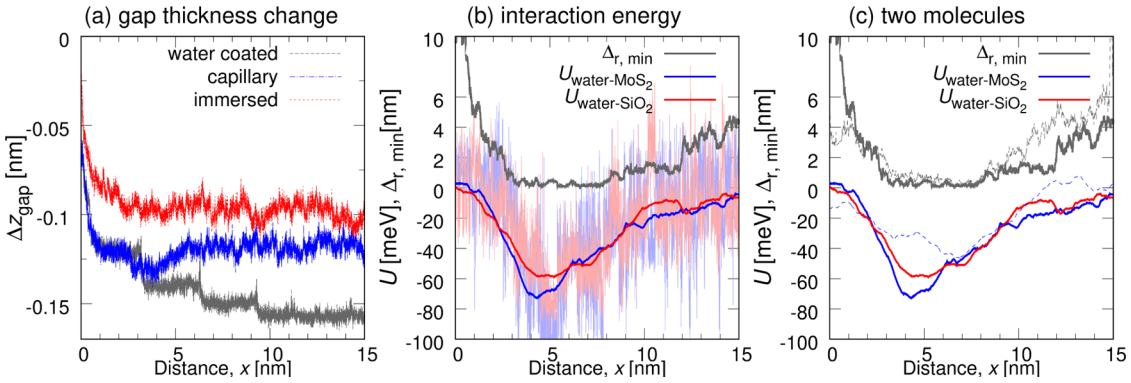

Figure 7. (a) Evolution of the Δz_{gap} gap thickness during a sliding simulation at an applied normal load of F_N = 17.3 nN in case of the three studied water setups along the *x*-axis. (b) The dependence of interaction energy (U) between a single water molecule and MoS_2 and SiO_2 surfaces and distance from energy minima $\Delta_{r,min}$ is given as the probe moves along the *x*-axis. The smoothed using moving average (bold lines) and raw numerical data (light lines) showing energy fluctuations are shown. (c) The evolution of dependence of interaction energy (U) is compared for two water molecules as the probe moves along the *x*-axis.

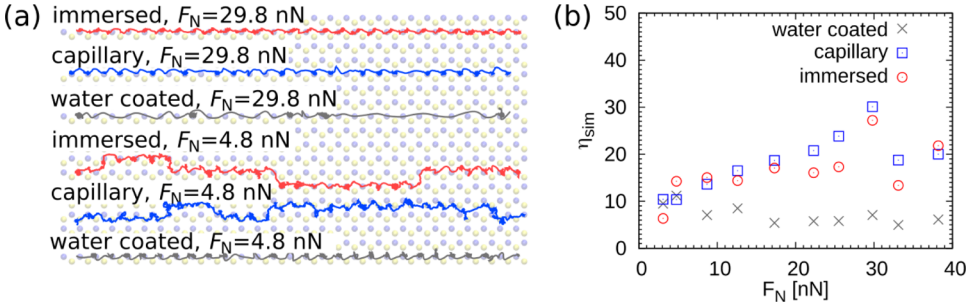

Figure 8. (a) Top views (*xy*- plane) of the trajectories of the center of mass of the water coated, surrounded by capillary water, and fully immersed probe's center of mass at applied loads of F_N = 4.8 nN and 29.8 nN. (b) PT model η_{sim} parameter determined in MD simulations.

identical probe-to-substrate distance. This indicates that the evolution of the center of mass *z*− position in Figure 7(a) results from the water molecules' presence in the probe-substrate contact. In both scenarios, whether the probe is immersed in a layer of water or surrounded by capillary water, the probe-to-substrate distance stabilizes after an initial descent. The eventual penetration of water molecules inside the sliding contact and their removal are dynamically balanced out. Therefore, it can be deduced that, when aiming to obtain high-resolution images using a water-based atomic force microscopy technique, a specific minimal value of the normal pressure is crucial for breaking the first hydration layer. After that, water molecules are not completely removed, but they behave as an integral part of the probe. The normal pressure necessary to break the first hydration layer is temperature-dependent, decreasing from 2.5 GPa at T = 280 K down to 1 GPa at T = 370 K, cf. Figure 5(b). Still, Figure 7(a) shows that the lattice resolved stick−slip motion is obtained with the capillary water. In a scenario where the probe is coated with a few water molecules, the close approach to the substrate results in exceptionally long slips. Conversely, the continuous water layer in the case of the probe immersed in water, causes an excessive separation between the probe and the substrate, thereby introducing a dynamic interference of water molecules into the stick−slip motion of the probe. It is important to note that changes in probe elevation and the geometry of the contact with the substrate in the experiment could also arise from various processes, such as the mobility of surface defects on the amorphous SiO_2 surface or tribochemical reactions between SiO_2 and water.[65,66]

Figure 7(b,c) illustrates the evolution of interaction energies (U) between single water molecule and MoS_2 and SiO_2 surfaces with sliding distance. The interaction energy values were derived from MD simulation data in Figure 7(a). These energies represent the combined effects of Coulombic and van der Waals forces between a single water molecule and the substrate/probe. While van der Waals forces are typically quite small, around 0.05 eV, Coulomb attractive forces dominate the present system. In Figure 7(b,c), the distance from the minima of this energy is also given ($\Delta_{r,min}$), so we can follow how the water molecule enters into the gap and leaves it. These results reveal that the interaction energies between water−solid surfaces are higher than thermal energy (ca. 30 meV) or energy of surface defects on SiO_2.[65] The interaction energy with MoS_2 approaches 80 meV, consistent with results, cf. ref 67. The distance of minimum shows that molecules can reside for an extended (about 6 nm) sliding distance in the tribological contact at one point due to stronger interactions with SiO_2 without chemically reacting with the surface.[66] We can also see by comparing two molecules that can move within their position taking different configurations with different interaction energies.

At this point, we focus on the effect of the normal load on the probe-substrate interaction, in the presence of water molecules. To better understand this problem, the center of mass trajectory in the substrate plane (*xy* plane) projected onto the MoS_2 plate, is visualized in Figure 8(a). The stick locations are seen as clumps at the Mo top sites, connected by curved slip paths between the S atoms. We performed a fast Fourier transform (FFT) on the lateral force for the F_N = 4.8

https://doi.org/10.1021/acsami.4c08226
ACS Appl. Mater. Interfaces 2024, 16, 44249−44260

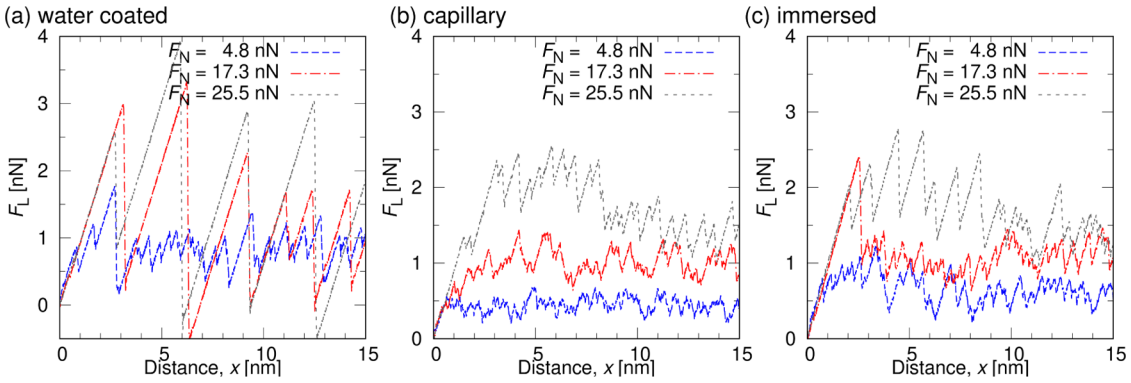

Figure 9. Representative lateral force traces, F_L acting on the probe which is sliding along the x-direction for (a) water coated probe, (b) surrounded by capillary water probe, and (c) fully immersed water probe. The lateral force traces are shown for the three normal forces F_N = 4.8, 17.3, and 25.5 nN. The sliding velocity was v_s = 2 m/s, while the spring stiffness was k = 1 N/m.

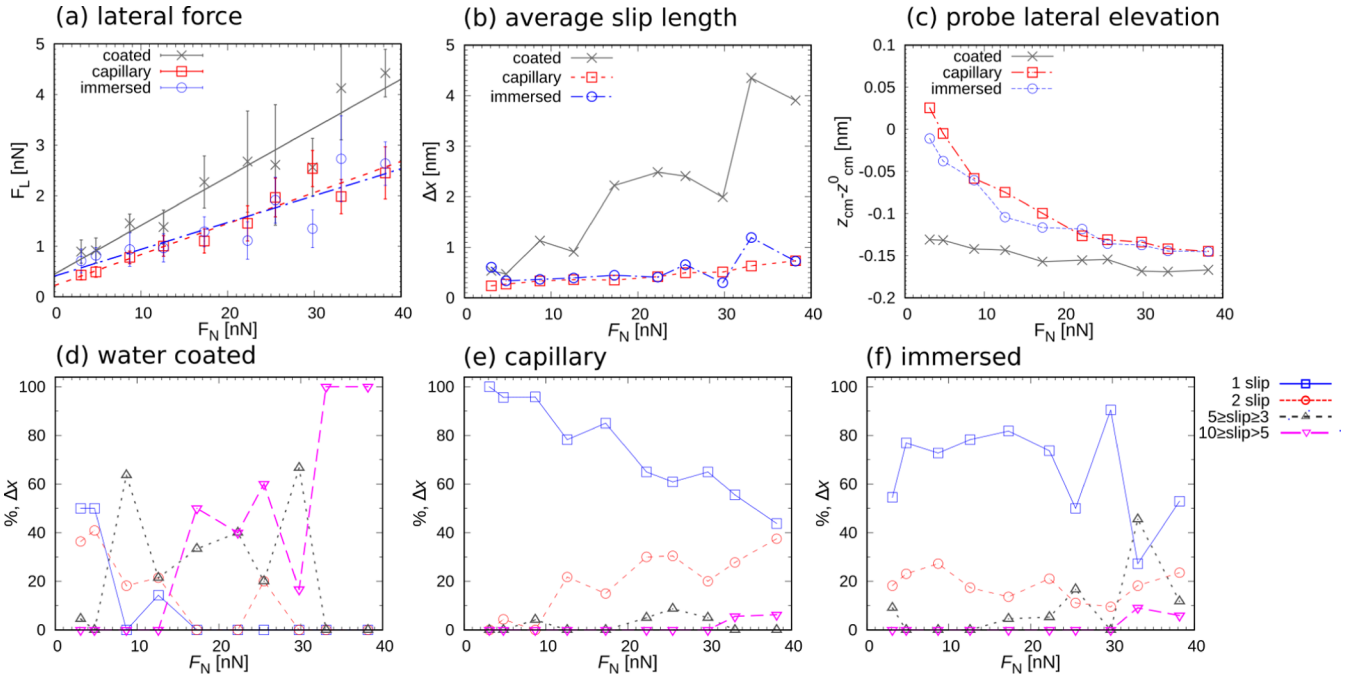

Figure 10. Simulated frictional behavior of SiO_2−MoS_2 tribosystem. Load dependence (F_N) in water coated (black), capillary (red), probe immersed in water (blue) of (a) average maximal lateral force (F_L), (b) average slip length Δx, and (c) probe's lateral elevation ($z_{cm} - z^0_{cm}$) after 15 nm of sliding. Percentage of the slip length populations of single slip events (denoted by blue continuous line), double slip events (red dashed), three to five lattice lengths (black dashed), and long jumps (cyan) are shown in panels (d) for water coated, (e) capillary, and (f) immersed probes, respectively.

nN normal load in all three systems, from which we resolved its underlying lattice periodicity which determines the single slip-length of ≈0.33 nm. Accordingly, the analysis of the dynamics and the distances between lateral force minima/maxima, indicates that the tip is immobilized at the hollow sites of MoS_2 monolayers (i.e., Mo top sites). Also from Figure 8(a), one can see that slip lengths correspond to the single or integer multiples of lattice from the in-plane position of the probe's center of mass projected onto the MoS_2 plate. The differences are striking when comparing normal loads of F_N = 4.8 and 29.8 nN, in both scenarios with abundant and scarce water. At low loads, the center of mass switches between different tracks, but at high loads the probe follows a single track when surrounded by a water capillary or immersed in water. This affects the lattice resolution and sometimes results in half-lattice-long constant slips. In the case of a water coated probe, we observe a single-track lattice resolved motion of the probe at a low load (F_N = 4.8 nN), while at a higher load (F_N = 29.8 nN), the slip paths are multiple lattice constants long.

Effect of the Normal Load on the Stick−Slip Friction in MD Simulations. Figure 9 presents the simulated lateral force traces of the system with (a) water coated probe, (b) probe surrounded by water capillary, and (c) probe immersed in a continuous layer of water. The traces are shown for the three normal forces of F_N = 4.8, 17.3, and 25.5 nN. We also calculated the PT parameter, like in the FFM experiment, to obtain insight into effective tip−sample sliding interaction, cf. Figure 8(b). The calculated η_{sim} at the different loads in Figure 8(b) shows an increase from ≈10 to ≈25 for capillary and layered water, and large fluctuations at F_N > 30 nN. Therefore, based on PT model observations, the corrugation interaction energy is greater than the elastic energy in these two systems.

https://doi.org/10.1021/acsami.4c08226
ACS Appl. Mater. Interfaces 2024, 16, 44249−44260

The PT parameter η_{sim} also evolves with increasing load, which is observed for the experimental PT parameter η_{exp} in ambient conditions. In the case of a water coated probe, the PT parameter is $\eta_{sim} \approx 6$ and does not depend on the applied normal load. In the case of a water coated probe, a lattice-resolved stick−slip friction pattern is obtained only at $F_N < 5$ nN, cf. Figure 9(a). At higher normal loads, i.e., 17.3, and 25.5 nN, we observe the multiple slip events. For all three systems, the averages of the maximal lateral force during the stick phase, are plotted in Figure 10(a). We extracted the friction coefficient and the zero-force of the water coated probe: $\mu_{coated} = 0.1 \pm 0.01$ and $F_{L,0} = 0.45 \pm 0.2$ nN, respectively. In the cases of the probe surrounded by capillary water, and the water-immersed probe, the friction coefficient is smaller: $\mu_{water} = 0.06 \pm 0.001$. The corresponding zero-force is $F_{L,0} = 0.31 \pm 0.1$ nN for the probe moving through the water layer.

All slopes, during the stick phase when the lateral force increases linearly with the sample's displacement, are similar and they are independent of the normal load, cf. Figure 9. The lateral stiffness calculated from the slopes is roughly 1 nN/nm, and therefore it is determined by the spring's stiffness which keeps the probe in place in both water-probe configurations.

We focus now on two important factors for lattice resolved stick−slip: the role of water in the contact region, and the impact of interactions between the probe and the surrounding water molecules (either in the capillary or water layer). As we already saw, the modeled system exhibits a stick−slip friction behavior even at the smallest investigated normal loads $F_N < 5$ nN, cf. Figure 9. The evolution of the average slip length in different environments is compared for different normal loads in Figure 10(b). In all three investigated systems, we observe a steady increase in the slip length with increasing normal load F_N. At the normal forces $F_N > 30$ nN, we observe the average slip lengths larger than 0.66 nm for immersed and capillary systems, cf. Figure 10(b). Still, even at $F_N < 40$ nN, high-resolution (lattice resolved) images are achievable in the full water layer. The increase of the average slip length with load is much larger for the water coated probe, cf. Figure 10(b). In the case of the water coated probe, the average slip length is larger than 3 nm for the normal forces $F_N > 30$ nN. A few water molecules trapped between the probe and the substrate can induce a slip with a lattice resolution in the case of a water coated probe only at the lowest investigated loads ($F_N < 5$ nN). Even under the normal force of $F_N = 8.7$ nN, the average slip length is larger than 1 nm.

Notably, the tip is not in direct contact with the surface in either of the three modeled systems. From Figure 10(c), we see that keeping the probe and the substrate somewhat separated increases the resolution of the measurements. Therefore, lattice resolved measurements become less sensitive to normal loads if the probe is immersed in a water layer or surrounded with water from a capillary. As a result, the FFM experiments could be conducted with a wider range of normal loads. Also, experimental measurements at higher normal loads can be performed. Both experimental conditions, the wider range and the inclusion of higher values of the applied normal load, improve the signal-to-noise ratio, which is advantageous.

To obtain a detailed insight into the evolution of the slip length in different configurations, we categorize the slip lengths into: single, double, three to five, and longer than five slip events, thus representing occurrences over one, two, three to five, or six and more lattice constants, respectively, along with the extent of these jumps in Figure 10(d−f). The probability of double (≈ 0.66 nm) and multiple-slip events is increasing in frequency at higher loads $F_N > 4.8$ nN. Figure 10(d−f) summarizes the evolution of the percentage of these slip events at varying applied normal loads for the three investigated systems. For the probe surrounded by a water capillary, there is a notable prevalence of the single-slip over the double-slip events, with the longer slip events being the least frequent. As the normal load increases, the portion of the single-slip events decreases from 100 to 50%, while the number of the double slips increases consequently, cf. Figure 10(e). In the case of the probe immersed in the water layer, the double-slip events are also present at low loads, i.e., $F_N < 5$ nN. The occurrence of double-slip events is around 20%. The three-slip population exhibits an intriguing behavior, initially being nonexistent, it is peaking at the lowest load $F_N = 25.5$ nN, subsequently declining to zero, and resurging at higher loads with approximately 40%, cf. $F_N = 33.1$ nN in Figure 10(f).

DISCUSSION

Analysis of the experimental data reveals distinct distributions in the measured slip lengths. Slip lengths exhibit characteristic distributions, with a notable prevalence of single-slip events under low loads in ambient conditions, compared to the probe immersed in water. Also in simulation, under low loads for the probe surrounded by capillary water, single-slip events are significantly more prevalent when compared to those observed for the probe fully immersed in water. The capillary simulation results above 10 nN align well with the experimental findings for ambient conditions, showing a shift from predominantly single-slip to double-slip events. Furthermore, both systems exhibit only single-slip and double-slip events. Similarly to the experiments, the simulations show an early presence of double-slip events in the water-immersed probe simulation. In addition, an interplay between the single-slip and double-slip events is observed with the normal load increase, for the water-immersed probe. That interplay is characterized by an initial decrease and subsequent increase in single-slip events, accompanied by a reciprocal trend in double-slip events, both in simulations and experiments.

The simulations allow investigation of cases that were not treated experimentally. The steep increase of the slip length and a high friction coefficient determined for the probe coated with a few water molecules (i.e., not enough water molecules to form a capillary) are seen in simulations. While single-slip and double-slip events dominate the experimental results, the simulations of the probe coated with water reveal a longer average slip length, which involves three or more slips. Also, the friction coefficient of $\mu_{coated} = 0.1$ for the probe coated with water is higher than both the experimentally observed value of 0.02 and the simulated value when an abundant amount of water is present, with the value of 0.06. Importantly, the discrepancy in the friction coefficient results suggests that the experimentally measured system under ambient conditions involved a probe surrounded by capillary water.

The simulations indicate that the presence of water extends the range of normal forces within which lattice-resolved resolution is achievable. Our analysis suggests that water molecules introduce interactions with energy levels between those of the thermally activated motion of amorphous SiO_2 probe surface defects (approximately 5−25 meV,[65]) and the elastic energies in the solids (probe/substrate), thereby enhancing the measurement sensitivity.

https://doi.org/10.1021/acsami.4c08226
ACS Appl. Mater. Interfaces 2024, 16, 44249−44260

The ratio between the tip−sample interaction and the cantilever elastic energy (i.e., the PT parameter η), increases by factor 3 in the ambient condition experiments, and by factor 2 in the simulations. The mean values of the corrugation interaction energy were larger than the elastic energy at the contacts in both experiments and simulations. At the same time, in the simulations of the water coated probe, the ratio η was independent of the normal load. Such a result further indicates that the trapped water molecules modify probe-substrate contact.

CONCLUSIONS

We have conducted extensive FFM experiments and MD simulations to investigate the structural, mechanical, and nanotribological properties of the studied nanoscale SiO_2/MoS_2 system in different aqueous environments. The simulation study focused on the interaction between an amorphous SiO_2 probe and a monolayer crystalline MoS_2 substrate, in the presence of three distinct configurations of water with respect to the probe: a water layer coating the probe and the probe-substrate gap, a sufficient amount of water surrounding the probe which enables the formation of a water capillary, and the probe fully immersed in a continuous layer of water. The experimental setup was 2-fold: an AFM probe immersed in a full layer of water and air with a relative humidity of 35−40%, where capillary condensation was a highly probable effect.

To understand the behavior of the water layer under the applied normal load and the breaking of the first hydration layer, we explored the vertical approach of the probe toward the substrate, and we obtained the force−distance characteristics at various temperatures. This molecular dynamics study revealed a significant influence of the temperature on the presence of water molecules within the probe-sample gap. Higher temperatures rendered the water molecules more mobile, resulting in fewer water molecules trapped in the probe-sample gap. However, both the heating of the system and the shear forces proved to be insufficient to expel the trapped water molecules.

Achieving lattice resolved images through water-based atomic force microscopy requires critical consideration of the minimal normal pressure needed to disrupt the initial hydration layer. Once this threshold is surpassed, the water molecules persist as integral components of the probe, rather than being entirely removed from the probe-sample gap.

The friction curves obtained via simulations and experiments exhibited well-defined lattice-resolved stick−slip patterns. Our MD simulations have explicitly revealed that the contact does not remain dry and that water molecules that get trapped become an integral factor in the overall nanotribological interaction. The simulations have shown that the slip length increases with the applied load to a prolonged stick−slip above 1 nm, when the amount of water surrounding the probe is low, as in the case of water coated probe. This result indicates that an abundance of water, either in the form of a capillary or water layer, allows the water molecules that get removed during sliding, to be replenished. In turn, the water trapped in the nanotribological probe-sample contact keeps the probe and sample separated further apart, compared to the dry case, or when the amount of water present is insufficient to form a capillary, hence resulting in the lattice resolution at the studied normal loads. By exploring the quantity and the spatial distribution of the water present in a nanoscopic contact of amorphous SiO_2 probe and monolayer MoS_2 sample, our combined simulation-experimental study contributes valuable insights into the intricate nature of the nanoscale tribological phenomena. Outlined phenomena involving trapped molecules may play an important role in nanotribological contact and have a strong impact on the quality and reliability of AFM measurements performed in liquid environments. However, open questions remain regarding the interaction of trapped water with surface SiO_2, particularly through hydroxylation and the interaction with surface defects. Additionally, given the anisotropic friction properties of MoS_2, further studies should investigate how does water influence this characteristic.

AUTHOR INFORMATION

Corresponding Authors

Miljan Dašić − *Scientific Computing Laboratory, Center for the Study of Complex Systems, Institute of Physics Belgrade, University of Belgrade, Belgrade 11080, Serbia;* orcid.org/0000-0002-1739-0784; Email: miljan.dasic@ipb.ac.rs

Ronen Berkovich − *Department of Chemical Engineering, Ben-Gurion University of the Negev, Beer Sheva 84105, Israel; The Ilse Katz Institute for Nanoscale Science and Technology, Ben-Gurion University of the Negev, Beer Sheva 84105, Israel;* orcid.org/0000-0002-0989-6136; Email: berkovir@bgu.ac.il

Igor Stanković − *Scientific Computing Laboratory, Center for the Study of Complex Systems, Institute of Physics Belgrade, University of Belgrade, Belgrade 11080, Serbia;* orcid.org/0000-0001-5756-7196; Email: igor.stankovic@ipb.ac.rs

Authors

Roy Almog − *Department of Chemical Engineering, Ben-Gurion University of the Negev, Beer Sheva 84105, Israel*

Liron Agmon − *Department of Chemical Engineering, Ben-Gurion University of the Negev, Beer Sheva 84105, Israel*

Stav Yehezkel − *Department of Chemical Engineering, Ben-Gurion University of the Negev, Beer Sheva 84105, Israel*

Tal Halfin − *Department of Chemical Engineering, Ben-Gurion University of the Negev, Beer Sheva 84105, Israel*

Jürgen Jopp − *The Ilse Katz Institute for Nanoscale Science and Technology, Ben-Gurion University of the Negev, Beer Sheva 84105, Israel*

Assaf Ya'akobovitz − *Department of Mechanical Engineering and The Ilse Katz Institute for Nanoscale Science and Technology, Ben-Gurion University of the Negev, Beer Sheva 84105, Israel;* orcid.org/0000-0002-5836-0549

Complete contact information is available at: https://pubs.acs.org/10.1021/acsami.4c08226

Notes

The authors declare no competing financial interest.

ACKNOWLEDGMENTS

M.D. and I.S. acknowledge funding provided by the Institute of Physics Belgrade, through the grant of the Ministry of Science, Technological Development and Innovation of the Republic of Serbia. R.B., L.A., R.A., and S.Y. acknowledge the support of the Pazy Foundation grant ID 133-2020, and Deutsche Forschungsgemeinschaft No. DFG GN 92/16-1. All computer simulations were performed on the PARADOX supercomputing facility at the Scientific Computing Laboratory of the Institute of Physics Belgrade, University of Belgrade, Serbia. The use of VMD[68] software for the visualization of our

https://doi.org/10.1021/acsami.4c08226
ACS Appl. Mater. Interfaces 2024, 16, 44249−44260

nanotribological system (available at http://www.ks.uiuc.edu/Research/vmd/) is also acknowledged.

REFERENCES

(1) de Beer, S.; Kutnyanszky, E.; Schön, P. M.; Vancso, G. J.; Müser, M. H. Solvent-induced immiscibility of polymer brushes eliminates dissipation channels. *Nat. Commun.* **2014**, *5*, No. 3781.
(2) Noël, O.; Mazeran, P.-E.; Stanković, I. Nature of Dynamic Friction in a Humid Hydrophobic Nanocontact. *ACS Nano* **2022**, *16*, 10768−10774.
(3) Wallace, A. G.; Symes, M. D. Water-splitting electrocatalysts synthesized using ionic liquids. *Trends Chem.* **2019**, *1*, 247−258.
(4) Feng, G.; Jiang, X.; Qiao, R.; Kornyshev, A. A. Water in Ionic Liquids at Electrified Interfaces: The Anatomy of Electrosorption. *ACS Nano* **2014**, *8*, 11685−11694.
(5) Fajardo, O. Y.; Bresme, F.; Kornyshev, A. A.; Urbakh, M. Water in Ionic Liquid Lubricants: Friend and Foe. *ACS Nano* **2017**, *11*, 6825−6831.
(6) Stanković, I.; Dašić, M.; Jovanović, M.; Martini, A. Effects of Water Content on the Transport and Thermodynamic Properties of Phosphonium Ionic Liquids. *Langmuir* **2024**, *40*, 9049−9058.
(7) Stella, M.; Lorenz, C. D.; Righi, M. C. Effects of intercalated water on the lubricity of sliding layers under load: a theoretical investigation on MoS2. *2D Mater.* **2021**, *8*, No. 035052.
(8) Arif, T.; Colas, G.; Filleter, T. Effect of humidity and water intercalation on the tribological behavior of graphene and graphene oxide. *ACS Appl. Mater. Interfaces* **2018**, *10*, 22537−22544.
(9) Zhao, X.; Zhang, G.; Wang, L.; Xue, Q. The tribological mechanism of MoS 2 film under different humidity. *Tribol. Lett.* **2017**, *65*, No. 64.
(10) He, G.; Müser, M. H.; Robbins, M. O. Adsorbed Layers and the Origin of Static Friction. *Science* **1999**, *284*, 1650−1652.
(11) Müser, M. H.; Robbins, M. O. Conditions for static friction between flat crystalline surfaces. *Phys. Rev. B* **2000**, *61*, 2335−2342.
(12) Müser, M. H.; Wenning, L.; Robbins, M. O. Simple Microscopic Theory of Amontons's Laws for Static Friction. *Phys. Rev. Lett.* **2001**, *86*, 1295−1298.
(13) Ouyang, W.; de Wijn, A. S.; Urbakh, M. Atomic-scale sliding friction on a contaminated surface. *Nanoscale* **2018**, *10*, 6375−6381.
(14) Bistac, S.; Schmitt, M.; Ghorbal, A.; Gnecco, E.; Meyer, E. Nano-scale friction of polystyrene in air and in vacuum. *Polymer* **2008**, *49*, 3780−3784.
(15) Yu, Y.; Cirelli, M.; Kieviet, B. D.; Kooij, E. S.; Vancso, G. J.; de Beer, S. Tunable friction by employment of co-non-solvency of PNIPAM brushes. *Polymer* **2016**, *102*, 372−378.
(16) Van den Oetelaar, R.; Flipse, C. Atomic-scale friction on diamond (111) studied by ultra-high vacuum atomic force microscopy. *Surf. Sci.* **1997**, *384*, L828−L835.
(17) Vilhena, J. G.; Pimentel, C.; Pedraz, P.; Luo, F.; Serena, P. A.; Pina, C. M.; Gnecco, E.; Pérez, R. Atomic-Scale Sliding Friction on Graphene in Water. *ACS Nano* **2016**, *10*, 4288−4293.
(18) Filleter, T.; Bennewitz, R. Structural and frictional properties of graphene films on SiC(0001) studied by atomic force microscopy. *Phys. Rev. B* **2010**, *81*, No. 155412.
(19) Goryl, M.; Budzioch, J.; Krok, F.; Wojtaszek, M.; Kolmer, M.; Walczak, L.; Konior, J.; Gnecco, E.; Szymonski, M. Probing atomic-scale friction on reconstructed surfaces of single-crystal semiconductors. *Phys. Rev. B* **2012**, *85*, No. 085308.
(20) Steiner, P.; Gnecco, E.; Krok, F.; Budzioch, J.; Walczak, L.; Konior, J.; Szymonski, M.; Meyer, E. Atomic-Scale Friction on Stepped Surfaces of Ionic Crystals. *Phys. Rev. Lett.* **2011**, *106*, No. 186104.
(21) Riedo, E.; Lévy, F.; Brune, H. Kinetics of Capillary Condensation in Nanoscopic Sliding Friction. *Phys. Rev. Lett.* **2002**, *88*, No. 185505.
(22) Pina, C. M.; Miranda, R.; Gnecco, E. Anisotropic surface coupling while sliding on dolomite and calcite crystals. *Phys. Rev. B* **2012**, *85*, No. 073402.
(23) Agmon, L.; Almog, R.; Gaspar, D.; Voscoboynik, G.; Choudhary, M.; Jopp, J.; Klausner, Z.; Ya'akobovitz, A.; Berkovich, R. Nanoscale contact mechanics of the interactions at monolayer MoS2 interfaces with Au and Si. *Tribiol. Int.* **2022**, *174*, No. 107734.
(24) Skuratovsky, S.; Agmon, L.; Gnecco, E.; Berkovich, R. Surroundings affect slip length dynamics in nanoscale friction through contact stiffness and damping. *Friction* **2023**, *11*, 216−227.
(25) Socoliuc, A.; Bennewitz, R.; Gnecco, E.; Meyer, E. Transition from stick-slip to continuous sliding in atomic friction: entering a new regime of ultralow friction. *Phys. Rev. Lett.* **2004**, *92*, No. 134301.
(26) Roth, R.; Glatzel, T.; Steiner, P.; Gnecco, E.; Baratoff, A.; Meyer, E. Multiple slips in atomic-scale friction: an indicator for the lateral contact damping. *Tribol. Lett.* **2010**, *39*, 63−69.
(27) Curry, J. F.; Argibay, N.; Babuska, T.; Nation, B.; Martini, A.; Strandwitz, N. C.; Dugger, M. T.; Krick, B. A. Highly Oriented MoS2 Coatings: Tribology and Environmental Stability. *Tribol. Lett.* **2016**, *64*, No. 11.
(28) Khare, H. S.; Burris, D. L. The Effects of Environmental Water and Oxygen on the Temperature-Dependent Friction of Sputtered Molybdenum Disulfide. *Tribol. Lett.* **2013**, *52*, 485−493.
(29) Winer, W. O. Molybdenum disulfide as a lubricant: a review of the fundamental knowledge. *Wear* **1967**, *10*, 422−452.
(30) Vazirisereshk, M. R.; Hasz, K.; Carpick, R. W.; Martini, A. Friction Anisotropy of MoS2: Effect of Tip−Sample Contact Quality. *J. Phys. Chem. Lett.* **2020**, *11*, 6900−6906.
(31) Xiao, X.; Qian, L. Investigation of humidity-dependent capillary force. *Langmuir* **2000**, *16*, 8153−8158.
(32) Ogletree, D. F.; Carpick, R. W.; Salmeron, M. Calibration of frictional forces in atomic force microscopy. *Rev. Sci. Instrum.* **1996**, *67*, 3298−3306.
(33) Varenberg, M.; Etsion, I.; Halperin, G. An improved wedge calibration method for lateral force in atomic force microscopy. *Rev. Sci. Instrum.* **2003**, *74*, 3362−3367.
(34) Irving, B. J.; Nicolini, P.; Polcar, T. On the lubricity of transition metal dichalcogenides: an ab initio study. *Nanoscale* **2017**, *9*, 5597−5607.
(35) Cao, X.; Gan, X.; Lang, H.; Yu, K.; Ding, S.; Peng, Y.; Yi, W. Anisotropic nanofriction on MoS2 with different thicknesses. *Tribiol. Int.* **2019**, *134*, 308−316.
(36) Almeida, C. M.; Prioli, R.; Fragneaud, B.; Cançado, L. G.; Paupitz, R.; Galvão, D. S.; De Cicco, M.; Menezes, M. G.; Achete, C. A.; Capaz, R. B. Giant and Tunable Anisotropy of Nanoscale Friction in Graphene. *Sci. Rep.* **2016**, *6*, No. 31569.
(37) Lee, C.; Li, Q.; Kalb, W.; Liu, X.-Z.; Berger, H.; Carpick, R. W.; Hone, J. Frictional Characteristics of Atomically Thin Sheets. *Science* **2010**, *328*, 76−80.
(38) Li, S.; Li, Q.; Carpick, R. W.; Gumbsch, P.; Liu, X. Z.; Ding, X.; Sun, J.; Li, J. The evolving quality of frictional contact with graphene. *Nature* **2016**, *539*, 541−545.
(39) Zeng, X.; Peng, Y.; Liu, L.; Lang, H.; Cao, X. Dependence of the friction strengthening of graphene on velocity. *Nanoscale* **2018**, *10*, 1855−1864.
(40) Xu, C.; Zhang, S.; Du, H.; Xue, T.; Kang, Y.; Zhang, Y.; Zhao, P.; Li, Q. Revisiting frictional characteristics of graphene: Effect of in-plane straining. *ACS Appl. Mater. Interfaces* **2022**, *14*, 41571−41576.
(41) Cho, D.-H.; Wang, L.; Kim, J.-S.; Lee, G.-H.; Kim, E. S.; Lee, S.; Lee, S. Y.; Hone, J.; Lee, C. Effect of surface morphology on friction of graphene on various substrates. *Nanoscale* **2013**, *5*, 3063−3069.
(42) Vazirisereshk, M. R.; Hasz, K.; Zhao, M.-Q.; Johnson, A. C.; Carpick, R. W.; Martini, A. Nanoscale friction behavior of transition-metal dichalcogenides: Role of the chalcogenide. *ACS Nano* **2020**, *14*, 16013−16021.
(43) Zhang, D.; Huang, M.; Klausen, L. H.; Li, Q.; Li, S.; Dong, M. Liquid-Phase Friction of Two-Dimensional Molybdenum Disulfide at the Atomic Scale. *ACS Appl. Mater. Interfaces* **2023**, *15*, 21595−21601.

(44) Zhang, S.; Hou, Y.; Li, S.; Liu, L.; Zhang, Z.; Feng, X.-Q.; Li, Q. Tuning friction to a superlubric state via in-plane straining. *Proc. Natl. Acad. Sci. U.S.A.* **2019**, *116*, 24452−24456.
(45) Gnecco, E.; Roth, R.; Baratoff, A. Analytical expressions for the kinetic friction in the Prandtl-Tomlinson model. *Phys. Rev. B* **2012**, *86*, No. 035443.
(46) Vega, C.; de Miguel, E. Surface tension of the most popular models of water by using the test-area simulation method. *J. Chem. Phys.* **2007**, *126*, No. 154707.
(47) Chatterjee, S.; Debenedetti, P. G.; Stillinger, F. H.; Lynden-Bell, R. M. A computational investigation of thermodynamics, structure, dynamics and solvation behavior in modified water models. *J. Chem. Phys.* **2008**, *128*, No. 124511.
(48) Sresht, V.; Rajan, A. G.; Bordes, E.; Strano, M. S.; Pádua, A. A.; Blankschtein, D. Quantitative Modeling of MoS2−Solvent Interfaces: Predicting Contact Angles and Exfoliation Performance using Molecular Dynamics. *J. Phys. Chem. C* **2017**, *121*, 9022−9031.
(49) Cruz-Chu, E. R.; Aksimentiev, A.; Schulten, K. Water-Silica Force Field for Simulating Nanodevices. *J. Phys. Chem. B* **2006**, *110*, 21497−21508.
(50) Allen, M. P.; Tildesley, D. J. *Computer Simulation of Liquids*; Oxford University Press, 2017.
(51) van Gunsteren, W. F. *Computer Simulation of Biomolecular Systems*; ESCOM Science Publishers BV, 1989.
(52) Plimpton, S. Fast parallel algorithms for short-range molecular dynamics. *J. Comput. Phys.* **1995**, *117*, 1−19.
(53) Pollock, E.; Glosli, J. Comments on P3M, FMM, and the Ewald method for large periodic Coulombic systems. *Comput. Phys. Commun.* **1996**, *95*, 93−110.
(54) Dumcenco, D.; Ovchinnikov, D.; Marinov, K.; Lazic, P.; Gibertini, M.; Marzari, N.; Sanchez, O. L.; Kung, Y.-C.; Krasnozhon, D.; Chen, M.-W.; et al. Large-area epitaxial monolayer MoS2. *ACS Nano* **2015**, *9*, 4611−4620.
(55) Medyanik, S. N.; Liu, W. K.; Sung, I.-H.; Carpick, R. W. Predictions and observations of multiple slip modes in atomic-scale friction. *Phys. Rev. Lett.* **2006**, *97*, No. 136106.
(56) Gnecco, E.; Agmon, L.; Berkovich, R. Friction and chaos: Influence of the damping coefficient on atomic-scale stick-slip on hexagonal crystal lattices. *Phys. Rev. B* **2022**, *105*, No. 235427.
(57) Helman, J. S.; Baltensperger, W.; Hol, J.; et al. Simple model for dry friction. *Phys. Rev. B* **1994**, *49*, No. 3831.
(58) Gnecco, E.; Bennewitz, R.; Gyalog, T.; Meyer, E. Friction experiments on the nanometre scale. *J. Phys.: Condens. Matter* **2001**, *13*, No. R619.
(59) Popov, V. L.; Gray, J. *Prandtl-Tomlinson Model: History and Applications in Friction, Plasticity, and Nanotechnologies*; Wiley Online Library, 2012; Vol. *92*, pp 683−708.
(60) Heyes, D. M.; Smith, E. R.; Dini, D.; Spikes, H. A.; Zaki, T. A. Pressure dependence of confined liquid behavior subjected to boundary-driven shear. *J. Chem. Phys.* **2012**, *136*, No. 134705.
(61) Perkin, S. Ionic liquids in confined geometries. *Phys. Chem. Chem. Phys.* **2012**, *14*, 5052−5062.
(62) Dašić, M.; Stanković, I.; Gkagkas, K. Molecular dynamics investigation of the influence of the shape of the cation on the structure and lubrication properties of ionic liquids. *Phys. Chem. Chem. Phys.* **2019**, *21*, 4375−4386.
(63) Gao, J.; Luedtke, W. D.; Landman, U. Layering Transitions and Dynamics of Confined Liquid Films. *Phys. Rev. Lett.* **1997**, *79*, 705−708.
(64) Suzuki, K.; Oyabu, N.; Kobayashi, K.; Matsushige, K.; Yamada, H. Atomic-Resolution Imaging of Graphite−Water Interface by Frequency Modulation Atomic Force Microscopy. *Appl. Phys. Express* **2011**, *4*, No. 125102.
(65) Xu, R.-G.; Zhang, G.; Xiang, Y.; Leng, Y. On the Friction Behavior of SiO2 Tip Sliding on the Au(111) Surface: How Does an Amorphous SiO2 Tip Produce Regular Stick−Slip Friction and Friction Duality? *Langmuir* **2023**, *39*, 6425−6432.
(66) Yeon, J.; van Duin, A. C. T.; Kim, S. H. Effects of Water on Tribochemical Wear of Silicon Oxide Interface: Molecular Dynamics (MD) Study with Reactive Force Field (ReaxFF). *Langmuir* **2016**, *32*, 1018−1026.
(67) Heiranian, M.; Wu, Y.; Aluru, N. R. Molybdenum disulfide and water interaction parameters. *J. Chem. Phys.* **2017**, *147*, No. 104706.
(68) Humphrey, W.; Dalke, A.; Schulten, K. VMD: visual molecular dynamics. *J. Mol. Graphics* **1996**, *14*, 33−38.

NOTE ADDED AFTER ASAP PUBLICATION

This paper originally published ASAP on August 6, 2024. As author Assaf Ya'akobovitz's name was incorrectly spelled in this version, this was corrected and a new version reposted on August 12, 2024.

https://doi.org/10.1021/acsami.4c08226
ACS Appl. Mater. Interfaces 2024, 16, 44249−44260